Calculation of the residual resistivity of three-dimensional quantum wires

T. N. Todorov
Department of Materials, University of Oxford, Parks Road, Oxford OX1 3PH, United Kingdom
(Received 31 January 1996; revised manuscript received 1 April 1996)

An exact scattering theory formulation of the elastic transport problem is used in a 1*s* tight-binding implementation to calculate the zero-temperature elastic resistances of disordered three-dimensional quantum wires with cross sections as large as 14×14 atoms and lengths of up to hundreds of atoms. A real-space Green function technique is used to construct the wires. The technique is flexible and simple to implement, making it possible to study a range of different geometries, types of disorder, and combinations thereof. The possible use of such calculations to evaluate the bulk residual resistivity of the respective materials is outlined. Attention is given to the statistics and the configurational averaging of the calculated results. The transition from the Ohmic to the localization regime in the wires is also studied. The shape of this transition, obtained from the numerical results, is found to correspond well to a curious semiempirical analytic form. Model calculations with different types of on-site disorder, and with interfacial roughness, combined with impurity scattering, are presented at the end. [S0163-1829(96)02732-4]

I. INTRODUCTION

Over the past two or three decades, the problem of electronic transport in phase-coherent disordered conductors has received intense attention, both theoretically and experimentally. On the theoretical side, direct numerical calculations have provided an important source of insight into the properties of such systems. Long thin conductors, sometimes referred to as quantum wires, have been a popular object of computational study. The simplest case of truly one-dimensional wires (e.g., a one-dimensional atomic chain) has been investigated in depth.[1] Two-dimensional wires (e.g., a planar atomic strip) have also been studied extensively. Recent numerical work includes studies of the density of states and of the localization lengths in such wires,[2,3] of the effect of disorder directly on the conductance and on the conductance quantization effect,[4] and of conductance fluctuations.[5,6]

The present paper is a report of calculations of the zero-temperature elastic (phonon-free) resistance of fully three-dimensional disordered quantum wires, with cross sections as large as 14×14 atoms and lengths of up to hundreds of atoms. The calculations employ a 1*s* tight-binding model[7] and are based on an exact single-particle scattering theory formulation of the elastic transport problem, presented and discussed elsewhere.[8] The calculation of the resistance for an individual wire involves a real-space Green function technique in which the Green function on a particular relevant interface in the system is calculated exactly in the disorder by a finite series of algebraic ''growth'' steps.[9,10,4] The method is applicable to one-, two-, and three-dimensional wires, and can be implemented with equal ease for a wide range of types of disorder.

The practical focus of this work is the possibility of using such calculations to evaluate the residual resistivity of the respective bulk material. The principle of the calculation is the following. A piece of disordered wire of cross section A and length L is connected to two perfect leads, and the resistance of the whole configuration is calculated. Configurational averaging is then performed in order to obtain a well-defined resistance R for that particular wire length, and the calculation is repeated for a series of lengths. The resistivity ρ for the respective bulk material is then found from the formula $\rho=As_O$, where s_O is the Ohmic slope of the calculated R versus L relation.

The two limitations of this procedure for obtaining the bulk resistivity are the deviations from Ohmic behavior in the wires due to localization effects, and the departures of the electronic properties of the wires from those of the true bulk. These limitations can, however, be overcome to some degree.

Consider first the problem of localization. According to a well-known argument,[11,12] the transition from the Ohmic regime, in which the resistance increases linearly with length, to the localization regime occurs at around that length of the wire for which the resistance reaches a value of one quantum resistance unit, $h/2e^2$. This length, the localization length ξ, is given by $\xi\sim(d/\lambda)^2 l$, where $d\sim\sqrt{A}$ is the characteristic transverse linear dimension of the wire, λ is the wavelength of the electrons, and l is the scattering mean free path. In a typical metal, λ is of the order of the interatomic spacing. Therefore, in a wire with a transverse linear dimension d of only a few atoms, ξ can be one or two orders of magnitude larger than l. Thus, even in a wire of nanometer dimensions, it may be possible to achieve a reasonable separation of the two regimes, with a sufficiently well-defined initial linear region to enable us to deduce the required Ohmic slope.

Consider next the problem of finite-size effects in the Ohmic regime. There are three separate such effects. First, the local density of states in the wire will not be the same as in the bulk. Secondly, the scattering properties of individual scatterers in the wire will not be the same as in the bulk. Thirdly, if reflections at the surface of the wire are nonspecular, then the scattering at the surface will contribute to the calculated resistance of the wire.[13,14] In a typical calculation, the wire would have a transverse linear dimension of, say, ten atoms. The Fermi wavelength of the electrons and the scattering cross section of a typical scatterer, say, an impurity atom, on the other hand, can be on the atomic scale.

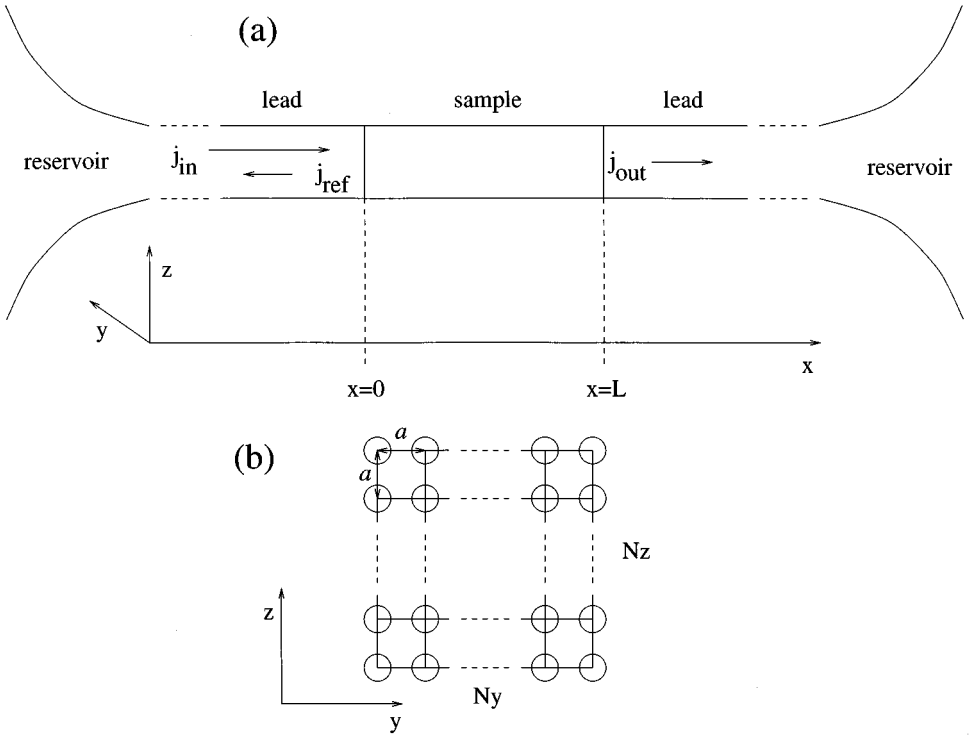

FIG. 1. (a) The general setup considered in the paper. The details are explained in the main text. (b) A typical (1,0,0) simple cubic atomic layer in the system, used for the numerical calculations. The lattice constant is a. There are N_y and N_z atoms along the y and z sides of the layer, respectively.

Also, often we will consider cases of very strong scattering, with mean free paths considerably smaller than the transverse wire dimension. It is then reasonable to hope that the calculated transport properties of the wire will be representative of, if not identical to, those of the true bulk.

An important advantage of the finite wire size is the possibility of treating the scattering by the disorder exactly. This type of calculation may be particularly valuable in the strong-scattering limit, when the use of conventional methods, such as those based on the Boltzmann equation or on the Kubo formula, can be difficult. Another useful feature of the present calculations is the possibility of studying *combinations* of different scattering mechanisms. One potential application of this type of calculation is in the study of the interplay between bulk and interfacial scattering in the giant magnetoresistance effect[15] in magnetic multilayers.

The idea of calculating the bulk resistivity ''by brute force,'' from the slope of the resistance versus length relation, has in the past been used in calculations on liquid and amorphous transition metals.[16] In those calculations, the resistance was obtained from the Landauer formula, after an explicit evaluation of the individual elements of the S matrix in k space, with periodic boundary conditions in the transverse directions.

In the present work we will use the real-space approach, mentioned earlier. Particular attention will be given to the problems of configurational averaging, the statistics of the calculated results, and the form of the transition from the Ohmic to the localization regime.

The rest of the paper is organized in the following way. The next section contains preliminary analytical estimates. Section III gives a description of the computational method. Section IV contains test calculations, aimed at investigating the general behavior of the results and at establishing a procedure for the configurational averaging. Section V is a study of two model examples—on-site disorder, and interfacial scattering without and with additional impurity scattering. Finally, Sec. VI contains a summary of the results, and a statement of several further lines of research.

II. PRELIMINARY ESTIMATES

The purpose of this section is to derive several relations, including an interesting formula for the transition between the Ohmic and the localization regime, which will be useful for the interpretation of the numerical results to be presented later on. To this end, we will carry out a classical kinetic evaluation of the Landauer formula for the two regimes.

The general setup considered in the paper is shown in Fig. 1(a). We have an infinite piece of wire of uniform cross section. The wire is a perfect conductor everywhere except for a single disordered segment of length L. This disordered segment will be referred to as the sample, and the semi-infinite pieces of perfect wire on both sides of it will be referred to as the leads. We imagine that somewhere ''at infinity'' each lead is connected through a smooth contact to an infinitely wide, macroscopic conductor, acting as an equilibrium particle reservoir. The zero-temperature conductance, with respect to a small electrochemical potential[17] difference *between the reservoirs*, of the whole configuration is given by the Landauer formula[18]

$$G = g \sum_k T_k , \tag{1}$$

where $g = 2e^2/h$ is the quantum conductance unit, the index k labels the open channels in a given lead, and T_k is the total transmission probability across the sample for an electron, incident upon it in the kth channel of the lead, at the Fermi energy.

Equation (1) can be written as

$$G = g\sum_k T_k = gN\frac{\sum_k T_k}{N} = gNT, \tag{2}$$

where N is the total number of open channels. The quantity $T=(\Sigma_k T_k)/N$ has the following meaning. Let, for definiteness, the left reservoir have the higher electrochemical potential. Then, within factors, N is the current $j_{\rm in}$, incident on the sample from the left reservoir. Within the same factors, $\Sigma_k T_k$ is the current $j_{\rm out}$, transmitted across the sample. Therefore $T=j_{\rm out}/j_{\rm in}$. In the rest of this section, we will be concerned with calculating T, thus defined.

A. Ohmic regime

First, we consider the situation in which the motion of the electrons in the disordered sample is purely diffusive, and evaluate the quantity $T=j_{\rm out}/j_{\rm in}$ for the case of classical diffusion. A steady incident current of electrons $j_{\rm in}$ is supplied into the left end of the sample. Some electrons diffuse through the sample into the right lead, giving rise to the transmitted current $j_{\rm out}$. The rest emerge back into the left lead, giving rise to a reflected current of magnitude $j_{\rm ref}$.

Let x be the longitudinal coordinate, with the left end of the sample at $x=0$ and the right end of the sample at $x=L$. In the steady state, the number of conducting electrons per unit length in the sample is given by $n(x)=A+Bx$, where the constants A and B are found from the boundary conditions as follows. At the right end of the sample there are only right-traveling electrons, emerging into the right lead. Thus we have $j_{\rm out}=n(L)v_x=-Dn'(L)$, where v_x is the average magnitude of the x component of velocity, and for the second equation we have used $j(x)=-Dn'(x)$, where $j(x)$ is the net current at position x in the sample and D is the diffusion coefficient. The density $n(0)$ at the left end of the sample is made up of the incident and the reflected electrons, emerging back into the left lead, giving $n(0)v_x=j_{\rm in}+j_{\rm ref}=2j_{\rm in}-j_{\rm out}$.

Writing $D=lv_x/2$, where l, to within a factor of order unity, is the mean free path, we easily find $T=j_{\rm out}/j_{\rm in}=1/(1+L/l)$. Substituting for T into Eq. (2), for the resistance $R=1/G$ *between the reservoirs* we obtain

$$R=R_0+R_0L/l, \tag{3}$$

where $R_0=r/N$, $r=1/g=h/2e^2$ being the quantum resistance unit.

R increases linearly with the length L of the sample through the second term,

$$R(L)=R_0L/l=rL/Nl. \tag{4}$$

This term gives the contribution of the disordered sample to the resistance of the system from Fig. 1(a). Equation (4) for the Ohmic resistance of a piece of disordered wire is a known and useful semiclassical relation.

To see the origin of the constant first term R_0 in Eq. (3), consider the case when there is no disordered region ($L=0$ or $l=\infty$), with $R=R_0$. Then the lead-sample-lead system constitutes a single piece of perfect conductor and the whole configuration represents a long ballistic contact between the two reservoirs. The resistance R_0 is thus analogous to the Sharvin resistance for a small aperture in an otherwise impenetrable barrier, and can be related conceptually to local voltage drops in the region of the contacts that connect the equilibrium reservoirs to the nonequilibrium leads.[19] The presence of the term R_0 in Eq. (3) reflects the fact that even if the conductor connecting the reservoirs is perfect, so long as this conductor has a finite cross section, it will carry a finite current for any finite electrochemical potential difference between the reservoirs.

Thus the resistance R between the reservoirs has an absolute minimum R_0 attained in the case of perfect transmission. Any net scattering in the conductor connecting the reservoirs manifests itself as a rise of R above R_0. In this paper we will study this rise as a function of the length of the disordered sample.

B. Localization regime

Fundamentally, localization in disordered media is a quantum interference effect.[20] According to a well-known argument,[11,12] in the presence of purely elastic scattering the electronic states in a thin wire are localized even when the bulk of the respective material is conducting. The corresponding localization length ξ is that length for which the classical resistance of the wire reaches a value of about $r=h/2e^2$.[11,12] Equation (4) then gives $\xi\sim Nl$, or, generally,

$$s_O\xi=rc, \tag{5}$$

where s_O is the slope of the resistance versus wire length in the Ohmic regime and c is a constant of order unity, which may depend on the cross section of the wire and on the disorder. For lengths larger than ξ, transmission across the disordered wire becomes exponentially small, and deep into the localization regime the resistance $R(L)$ of the wire increases exponentially with length as $R(L)\sim\exp(L/\xi)$.

Consider now the question of how the Ohmic regime, with $R(L)=s_OL$, evolves into the localization regime. Since $s_O=rc/\xi$, the Ohmic regime could be seen as the initial part of the exponential $rc\exp(L/\xi)$. Indeed, for a one-dimensional system[21] one has $R(L)=r[\exp(L/\xi)-1]$. For a wire of finite cross section,[22,23] this relation could be extended to $R(L)=rc[\exp(L/\xi)-1]$, or $R=rc[\exp(L/\xi)-1]+R_0$ for the resistance between the reservoirs. However, the relation $R(L)=rc[\exp(L/\xi)-1]$ predicts a faster departure from the Ohmic line $R(L)=s_OL=rcL/\xi$ than is seen in the calculations to be presented later on. The results of these calculations fit another relation, which will be obtained below in an empirical way.

Consider the following physical argument. For a system with one open channel the relation $\xi\sim Nl$ reduces to $\xi\sim l$. Thus, in one dimension, the localization length is similar to the mean free path. The motion of the electron on the scale of the localization length is essentially *ballistic*. The electron is trapped between two neighboring scatterers and bounces between them like a particle in a box, not ''forgetting'' even for a moment that it is localized. But in a wire with a large number of open channels, $\xi\gg l$ and the electron motion over lengths $L<\xi$ is *diffusive*. Most of the time the electron struggles along in its diffusive propagation, and only occasionally, when it manages to cover a net distance of ξ, does it have occasion to realize that it is in fact localized. It is then

tempting to think that Ohm's law will hold over a greater *fraction* of the localization length than in the case $N=1$. In other words, $R(L)$ may be expected to increase more slowly with L than the function $rc[\exp(L/\xi)-1]$, with a longer initial linear region.

Here, we will not seek a detailed treatment[24] of the scaling with length of the transmission probabilities $\{T_k\}$ in the Landauer formula. Instead, we consider a classical kinetic model, based on the above considerations. We imagine that in addition to the disorder, giving rise to the scattering of mean free path l, the sample from Fig. 1(a) contains a random distribution of traps, which occasionally capture the diffusing electrons. Let us recalculate the quantity $T=j_{\rm out}/j_{\rm in}$.

In the presence of the trapping, the steady-state diffusion equation is modified by a sink term, and reads $n''(x)-\eta^2 n(x)=0$, where η is an effective inverse trapping length. We have assumed that $\eta l \ll 1$, so that the relation $j(x)=-Dn'(x)$, and hence the linear diffusion equation, holds. The solution for the linear density is $n(x)=A\exp(\eta x)+B\exp(-\eta x)$, where A and B are fitted to the boundary conditions as before but with $j_{\rm ref}=j_{\rm in}-j_{\rm out}-j_{\rm trap}$, where $j_{\rm trap}=D\eta^2\int_0^L n(x)\,dx$ is the total rate of capture of electrons in the sample. The trapping length is set equal to the localization length, $\eta=1/\xi$. With $D=lv_x/2$, the resistance $R=1/(gNT)$ between the reservoirs becomes

$$R=r[c\sinh(L/\xi)+(1/N)\cosh(L/\xi)], \tag{6}$$

where, by definition, $c=s_O\xi/r$ and the effective Ohmic slope s_O is given by $s_O=R_0[1+(l/2\xi)^2]/l$, with $R_0=r/N$. In the limit $L/\xi \ll 1$, Eq. (6) gives the Ohmic line $R=s_O L+R_0$. Comparison with the case of pure diffusion, Eq. (3), shows that the slope s_O has picked up an ''echo'' from the presence of the trapping and differs from its old value by a fractional amount of $(l/2\xi)^2$. This fractional difference is of order $(1/N)^2$, and for $N>10$ it is less than 1%.

For $c=1$, $N=1$ Eq. (6) reproduces the result $R=r\exp(L/\xi)$ for the resistance between the reservoirs for a one-dimensional wire. In the limit $N\gg 1$, which is the case of interest here, Eq. (6) can be approximated by replacing $\cosh(L/\xi)$ by unity, giving the asymptotic form

$$R=R_0+rc\sinh(L/\xi). \tag{7}$$

The contribution $R(L)$ of the disordered sample is given by the L-dependent term,

$$R(L)=rc\sinh(L/\xi). \tag{8}$$

Equation (8) and the possible relation $R(L)=rc[\exp(L/\xi)-1]$, mentioned earlier, produce the same initial Ohmic slope and the same slope of $\ln[R(L)]$ versus L in the region $L/\xi \gg 1$. However, the relation $R(L)=rc[\exp(L/\xi)-1]$ gives a faster rise above the Ohmic line $R(L)=rcL/\xi$ than Eq. (8). Also, in the region $L/\xi \gg 1$ the two expressions differ by a factor of 2.

Equations (7) and (8) have been derived for the case of classical diffusion through a disordered wide sample ($N\gg 1$) in the presence of an additional trapping mechanism. There is no *a priori* reason to expect that these results should be relevant to the true quantum-mechanical problem. Nonetheless, the above equations fit the numerical results very well, for a range of wire cross sections and types of disorder. In particular, for a given initial slope s_O and for a given localization length ξ, obtained after appropriate averaging, the above equations produce a good fit to the numerical data both in the Ohmic and in the localization regime.

Here, we leave this observation without further comment, on the understanding that even if the above results capture something essential about the true problem, these results require further and independent justification. Instead, here we treat these results as empirical relations, and use them to set limits on what is to be regarded as the Ohmic region in the calculations.

For $L/\xi<1$, we have $\sinh(L/\xi)\approx(L/\xi)[1+(1/6)(L/\xi)^2]$. Taking 1% as the level of tolerance for departures from linearity sets $L/\xi<1/4$, which with $R(L)=s_O L=rcL/\xi$ gives $R(L)<rc/4$. Since c is of order unity, within the 1% tolerance level the Ohmic region is to be treated as that region in which the resistance of the sample is less than about 1/4 in units of $r=h/2e^2$. This estimate applies also to the resistance R between the reservoirs, since once $R(L)$ becomes comparable to r, with $N\gg 1$ the term $R_0=r/N$ in Eq. (3) becomes negligible.

Since $\xi\sim Nl$, the condition $L/\xi<1/4$ gives $L/l<N/4$. In a typical calculation, we will have $N\sim 60$, so that $L/l<15$. Thus the present bulk resistivity studies are limited to wire lengths that exceed the mean free path by about one order of magnitude. The limit $l/L\ll 1$ can be approached by increasing the wire cross section, and hence N. The limitations in doing so are computational.

III. METHOD FOR THE CALCULATION OF THE RESISTANCE

This section contains a statement of the method for the calculation of the resistance for an individual wire. In the present calculations, the sample and the two semi-infinite perfect leads are given the same simple cubic lattice structure of lattice parameter a. The whole infinite wire is an array of identical rectangular (1,0,0) atomic layers, stacked along the longitudinal [100] direction, namely, the x axis. The transverse y and z axes, in the plane of these layers, are along the [010] and [001] directions, respectively. Each atomic layer has N_y atoms along the y axis and N_z atoms along the z axis [Fig. 1(b)]. The number of (1,0,0) layers in the sample specifies the length L of the sample, in units of the lattice parameter a. The electronic structure of the whole system is described by an orthonormal nearest-neighbor $1s$ tight-binding model with an ideal hopping integral γ and an on-site energy on the native atoms (e.g., the atoms in the perfect leads) of zero. The calculation of the resistance for the whole lead-sample-lead system is done by an extension of a method used previously in work on two-dimensional wires.[4] The calculation consists of three steps which are described below.

A. The surface Green function for the bare semi-infinite perfect lead

The first step is to find the matrix elements of the Green function for the bare perfect semi-infinite lead between atomic sites in the end, free layer of the lead. The method for

calculating these matrix elements is an extension of a method used previously in work on two-dimensional wires.[4,10]

Consider the left lead. The lead is an array of identical rectangular (1,0,0) atomic layers, stacked along the longitudinal [100] direction (the x axis). Let us number these layers from 1 to ∞, with layer 1 being the end, free layer. Each atomic layer in isolation has a set of orthonormal eigenstates $\{|\mathbf{p}\rangle\}$, given by

$$|\mathbf{p}\rangle=\left(\frac{2}{N_y+1}\right)^{1/2}\left(\frac{2}{N_z+1}\right)^{1/2}\times\sum_{n_y=1}^{N_y}\sum_{n_z=1}^{N_z}\sin\left(\frac{p_y n_y\pi}{N_y+1}\right)\sin\left(\frac{p_z n_z\pi}{N_z+1}\right)|\mathbf{n}\rangle. \tag{9}$$

Here, $\mathbf{n}$ designates the pair of integers (n_y,n_z). The integers n_y and n_z label an atom in the layer, in an obvious notation, and $|\mathbf{n}\rangle$ is the $1s$ state on that atom. The symbol $\mathbf{p}$, which labels the eigenstates for the whole layer, designates the pair of integers (p_y,p_z), with $p_y=1,\ldots,N_y$ and $p_z=1,\ldots,N_z$. The layer states $\{|\mathbf{p}\rangle\}$ have energies $\{E(\mathbf{p})\}$, given by

$$E(\mathbf{p})=-2|\gamma|\cos\left(\frac{p_y\pi}{N_y+1}\right)-2|\gamma|\cos\left(\frac{p_z\pi}{N_z+1}\right). \tag{10}$$

Now let $|l,\mathbf{p}\rangle$ be the respective layer state on the lth atomic layer in the semi-infinite perfect lead. Let H be the Hamiltonian for the lead. The matrix element $\langle l,\mathbf{p}|H|m,\mathbf{p}'\rangle$ is not identically equal to zero only if $\mathbf{p}=\mathbf{p}'$. For the case $\mathbf{p}=\mathbf{p}'$, we denote this matrix element by $H_{lm}(\mathbf{p})$ and note that if $l=m$, then $H_{lm}(\mathbf{p})=E(\mathbf{p})$, if $l=m\pm1$, then $H_{lm}(\mathbf{p})=\gamma$, and finally, if $l\neq m$ and $l\neq m\pm1$, then $H_{lm}(\mathbf{p})=0$. Let $G^{0+}(E)$ be the retarded Green function for the lead. Like H, $G^{0+}(E)$ is diagonal in the label $\mathbf{p}$. Let $G^{0+}_{lm}(E,\mathbf{p})$ stand for the matrix element $\langle l,\mathbf{p}|G^{0+}(E)|m,\mathbf{p}\rangle$.

Now imagine appending another layer to the end of the semi-infinite lead. Let this layer have index 0. We imagine that this new layer is bonded to the lead perfectly, so that the new lead is geometrically identical to the old lead. The bonding of the new layer to the lead is realized by a term V in the Hamiltonian, whose only nonzero matrix elements in the basis of layer states $\{|l,\mathbf{p}\rangle\}$ are $V_{01}(\mathbf{p})=V_{10}(\mathbf{p})=\gamma$. We also have $G^{0+}_{00}(E,\mathbf{p})=1/[E-E(\mathbf{p})+i\epsilon]$, where $\epsilon\to0^+$, and $G^{0+}_{0l}(E,\mathbf{p})=G^{0+}_{l0}(E,\mathbf{p})=0$ for all $l\neq0$.

Let $G^{+}(E)$ be the Green function for the lead with the new layer bonded to it. Solving the Dyson equation

$$G^{+}(E)=G^{0+}(E)+G^{0+}(E)VG^{+}(E) \tag{11}$$

we easily find

$$G^{+}_{00}(E,\mathbf{p})=\frac{1}{|\gamma|}\,\frac{\mathcal{E}-\mathcal{E}(\mathbf{p})\pm\sqrt{[\mathcal{E}-\mathcal{E}(\mathbf{p})]^2-4}}{2}, \tag{12}$$

where $\mathcal{E}=E/|\gamma|$, $\mathcal{E}(\mathbf{p})=E(\mathbf{p})/|\gamma|$, and we choose the solution with the minus sign if the expression under the square root is negative, while if this expression is positive, we choose the solution with the minus sign if $[\mathcal{E}-\mathcal{E}(\mathbf{p})]>0$ and the solution with the plus sign if $[\mathcal{E}-\mathcal{E}(\mathbf{p})]<0$. The rules for choosing between the two solutions have been discussed elsewhere.[4,8,10]

Consider now two atomic sites $\mathbf{m}$ and $\mathbf{n}$ in the end layer of the lead. We require the matrix element of $G^{+}(E)$ between them. Call this matrix element $G^{+}(E;\mathbf{m},\mathbf{n})$. We have

$$\begin{aligned}G^{+}(E;\mathbf{m},\mathbf{n})&=\langle\mathbf{m}|G^{+}(E)|\mathbf{n}\rangle\\&=\sum_{k,l,\mathbf{p}}\langle\mathbf{m}|k,\mathbf{p}\rangle G^{+}_{kl}(E,\mathbf{p})\langle l,\mathbf{p}|\mathbf{n}\rangle\\&=\sum_{\mathbf{p}}\langle\mathbf{m}|0,\mathbf{p}\rangle G^{+}_{00}(E,\mathbf{p})\langle0,\mathbf{p}|\mathbf{n}\rangle\end{aligned} \tag{13}$$

or, using Eq. (9) for $|0,\mathbf{p}\rangle$,

$$G^{+}(E;\mathbf{m},\mathbf{n})=\left(\frac{2}{N_y+1}\right)\left(\frac{2}{N_z+1}\right)\times\sum_{\mathbf{p}}\sin\left(\frac{p_y m_y\pi}{N_y+1}\right)\sin\left(\frac{p_z m_z\pi}{N_z+1}\right)\times\sin\left(\frac{p_y n_y\pi}{N_y+1}\right)\sin\left(\frac{p_z n_z\pi}{N_z+1}\right)G^{+}_{00}(E,\mathbf{p}). \tag{14}$$

The above expression for the matrix element $G^{+}(E;\mathbf{m},\mathbf{n})$ of the Green function between sites $\mathbf{m}$ and $\mathbf{n}$ in the end atomic layer of the semi-infinite lead can be evaluated by hand.

B. Growth of the sample

The next step in the calculation consists in growing the sample, layer by layer, onto the left lead.[9] The implementation is the same as in earlier work on two-dimensional wires,[4] and here the growth sequence will be described only briefly. In the first step of the growth sequence, the first atomic layer of the sample is bonded to the end layer of the left lead. In the second growth step, the second layer of the sample is bonded to the first layer, and so on. At every step the Green function matrix elements between atomic sites in the last added layer are calculated by solving numerically the Dyson equation, Eq. (11). For a typical growth step, the quantities $G^{0+}(E)$, V, and $G^{+}(E)$ are constructed in the following way. $G^{0+}(E)$ is the Green function for the situation just before the growth step. In this situation, the atoms of the layer that is to be added are not yet bonded to each other or to the atoms in the previous layer. The matrix elements of $G^{0+}(E)$ between atoms in the previous layer are available from the previous growth step. The only other nonzero matrix elements of $G^{0+}(E)$ are the on-site matrix elements on the atoms in the new layer. These matrix elements are given by $1/(E-E_{\text{atom}})$, where E_{atom} is the on-site energy on the respective atom in the new layer. The term V describes the bonding of atoms in the new layer to each other and to atoms in the previous layer. The bonding extends to nearest neighbors only. Finally, $G^{+}(E)$ is the Green function for the situation just after the growth step, with the new layer fully bonded to the previous layer. The growth sequence is continued up to and including the last atomic layer of the sample. In this situation there still is no bonding between the last layer of the sample and the right lead.

C. Calculation of the resistance

In the situation at the end of the growth sequence, which will now be referred to as the initial situation, the system consists of two decoupled semi-infinite systems. One of them, system 1, is the left lead with the sample fully grown on to it, and the other, system 2, is the right lead.

Let $G^{0\pm}(E)$ now be the retarded and advanced Green functions for the initial situation with $G^{0-}(E)=[G^{0+}(E)]^{\dagger}$. The matrix elements of $G^{0+}(E)$ between atoms in the last layer of the sample and between atoms in the first layer of the right lead are available from the previous stages of the calculation, while those between an atom in the sample and an atom in the right lead are all zero.

Let $G_1^{0\pm}(E)$ and $G_2^{0\pm}(E)$ be the projections of $G^{0\pm}(E)$ onto systems 1 and 2, respectively. Thus if m and n are two atomic sites then the matrix element $\langle m|G_1^{0\pm}(E)|n\rangle$ is equal to $\langle m|G^{0\pm}(E)|n\rangle$ if m and n are both in system 1, and is zero otherwise, and analogously for $G_2^{0\pm}(E)$. It will be convenient to write $G_1^{0\pm}(E)$ and $G_2^{0\pm}(E)$ in the following way. Let $\{|1\rangle\}$ be all $1s$ atomic basis states in system 1 and let $\{|2\rangle\}$ be all $1s$ atomic basis states in system 2. Let us introduce the projection operators $P_1=\Sigma_1|1\rangle\langle 1|$ and $P_2=\Sigma_2|2\rangle\langle 2|$. Then, $G_1^{0\pm}(E)=P_1G^{0\pm}(E)=G^{0\pm}(E)P_1$ and $G_2^{0\pm}(E)=P_2G^{0\pm}(E)=G^{0\pm}(E)P_2$.

Let $d_1^0(E)$ and $d_2^0(E)$ be the density of states operators for systems 1 and 2, respectively, defined by

$$d_j^0(E)=\frac{1}{2\pi i}[G_j^{0-}(E)-G_j^{0+}(E)], \quad j=1,2. \tag{15}$$

In the geometry from Fig. 1(a), which now will be referred to as the final situation, systems 1 and 2 are fully bonded together. Let $G^{\pm}(E)$ be the retarded and advanced Green functions for the final situation. The transition from the initial to the final situation is realized by the addition to the initial Hamiltonian of a term V, containing the hopping integrals between systems 1 and 2.

As has been shown previously,[8] the zero-temperature conductance G of the geometry in the final situation is given by

$$G=g\ 4\pi^2\mathrm{Tr}[d_1^0(E_F)t^{\dagger}(E_F)d_2^0(E_F)t(E_F)], \tag{16}$$

with spin degeneracy included in the prefactor of the trace. In the above equation, E_F is the Fermi energy and the operator $t(E)$ is given by

$$t(E)=V+VG^{+}(E)V, \tag{17}$$

which, from Eq. (11), can also be written as

$$t(E)=V+VG^{0+}(E)t(E). \tag{18}$$

The conductance in Eq. (16) is the same[8] as what was defined in Sec. II as the conductance *between the reservoirs*. Equation (16) is simply an explicit form for the Landauer formula, Eq. (1).

Equation (16) can be evaluated by taking the trace in the positional $1s$ basis after solving Eq. (18) numerically to find $t(E)$. However, this method of evaluation turns out to be highly expensive computationally. The reason is that the trace in Eq. (16) involves four independent summations, over four separate sets of atomic indices. Each set of indices contains a number of elements equal to the number (N_yN_z) of atoms in the cross section of the wire and the computer time taken to sum all the terms in the trace grows as $(N_yN_z)^4$. This last stage of the calculation rapidly overtakes the actual growth sequence, the computer time for which grows as $(N_yN_z)^3$, and soon makes the calculation impossible.

This problem can be solved by writing Eq. (16) in another, equivalent form, the evaluation of which, however, is much faster. Let us first write Eq. (16) in the following symmetric form:

$$G=g\ 2\pi^2\{\mathrm{Tr}[d_1^0(E_F)t^{\dagger}(E_F)d_2^0(E_F)t(E_F)] + \mathrm{Tr}[d_2^0(E_F)t^{\dagger}(E_F)d_1^0(E_F)t(E_F)]\}. \tag{19}$$

The two terms in the right hand side of the above equation are equal to each other. In the case of the present $1s$ tight-binding model, their equality follows from the fact that $G^{0\pm}(E)$ and V, and hence $G^{\pm}(E)$ and $t(E)$, are symmetric matrices in the atomic basis. However, they are also equal to each other generally, as a consequence of an earlier result,[8] based on the optical theorem from scattering theory.

Let $d(E)$ be the density of states operator for the final situation, given by

$$d(E)=\frac{1}{2\pi i}[G^{-}(E)-G^{+}(E)]. \tag{20}$$

Let I be the operator for the particle current between systems 1 and 2, given by[8]

$$I=\frac{1}{i\hbar}(P_2V-VP_2), \tag{21}$$

where P_1 and P_2 are the two projection operators defined earlier. Equation (19) is then equivalent to

$$G=g\ 2\pi^2\hbar^2\mathrm{Tr}[d(E_F)Id(E_F)I]. \tag{22}$$

The equivalence of Eqs. (19) and (22) for G can be established by tedious but simple algebra. This is done in the Appendix. The structure of Eq. (22) is familiar from linear response theory.[9]

Since $P_1+P_2=1$, Eq. (21) can also be written as $I=(1/i\hbar)(P_2VP_1-P_1VP_2)$. V bonds the last layer of the sample to the first layer of the right lead. The only nonzero matrix elements of V in the atomic basis therefore are those between an atom in the sample and the atom *right opposite it*, in the right lead. Hence, if I_{ij} is a matrix element of the current operator, then specifying the index i (j) fixes j (i). Therefore the evaluation of the trace in Eq. (22) involves only two summations, over two separate sets of atomic indices, and the time required to sum the terms in this trace scales only as $(N_yN_z)^2$.

Finally, the conductance G between the reservoirs is calculated from Eq. (22) after solving the Dyson equation to find $G^{\pm}(E_F)$ for the final situation from $G^{0\pm}(E_F)$ for the initial situation. The respective resistance between the reservoirs is then found from $R=1/G$.

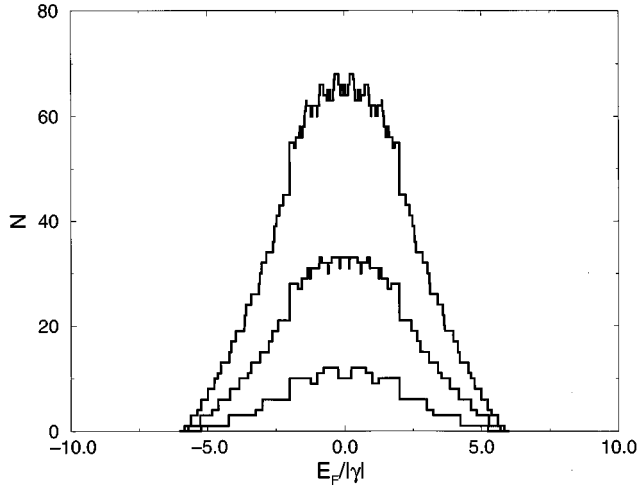

FIG. 2. The number of open channels N versus the Fermi energy E_F in units of $|\gamma|$ for perfect wires with cross section of 4×4 atoms (bottom plot), 7×7 atoms (middle plot), and 10×10 atoms (top plot).

IV. TEST CALCULATIONS

This section contains calculations aimed at showing the general behavior of the results, establishing a procedure for the configurational averaging, studying the transition from the Ohmic to the localization regime, and testing the convergence of the estimated bulk resistivity as a function of wire cross section, for a particular case.

A. Electronic structure of the perfect wire

First, consider the $1s$ band structure of the infinite perfect wire. In the absence of disorder each layer state, Eq. (9), gives rise to a subband of freely propagating wire states. The subband arising from layer state $|\mathbf{p}\rangle$ is centered on the energy $E(\mathbf{p})$, Eq. (10), and extends from $E(\mathbf{p})-2|\gamma|$ to $E(\mathbf{p})+2|\gamma|$. The subbands that cross the Fermi energy E_F specify the open conduction channels. Figure 2 shows plots of the number of open channels N as a function of $E_F/|\gamma|$ for wires with cross section of 4×4 atoms, 7×7 atoms, and 10×10 atoms. As the cross section increases, N increases in magnitude, while the shape of the plots follows the $1s$ bulk density of states for the infinite perfect simple cubic crystal.[25] The $1s$ band for the infinite crystal with zero on-site energy extends from $-6|\gamma|$ to $+6|\gamma|$. The steps on each plot are the same as the quantization steps in the ballistic conductance.

B. Configurational averaging

Now we turn to disordered wires. In this subsection we define a procedure for the configurational averaging of the results. We consider on-site disorder. The hopping integrals in the sample are the same as in the perfect leads (γ). The on-site energy on every sample atom is set randomly to $+E_a$ or $-E_a$, producing a 50-50 random substitutional alloy. The wire cross section is 8×8 atoms. E_a is set to $1.1|\gamma|$. The Fermi energy is set to $E_F=-0.1|\gamma|$, close to the middle of the band. The number of open channels in the perfect wire is $N=43$.

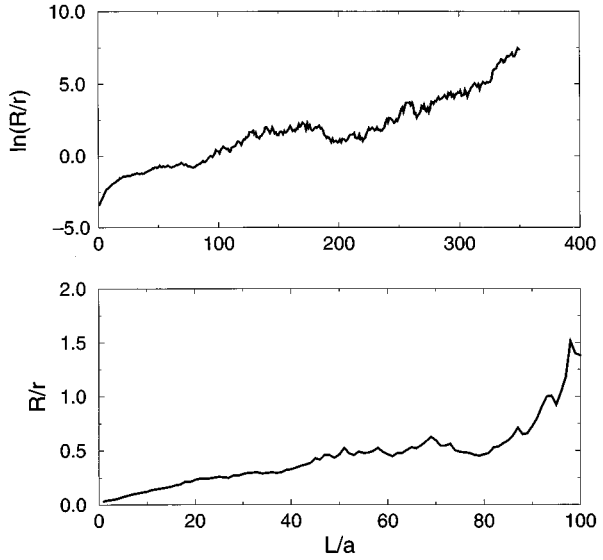

FIG. 3. R in units of $r=h/2e^2$ (lower panel) and $\ln(R/r)$ (upper panel) versus sample length L in units of a. The wire cross section is 8×8 atoms and $E_F=-0.1|\gamma|$ with $N=43$. The sample has random on-site energies of $\pm1.1|\gamma|$.

Before carrying out an actual calculation, let us estimate the mean free path l, the Ohmic slope s_O, and the localization length ξ in the disordered sample. Treating each sample atom as an independent weak isotropic scatterer of scattering potential $V=\pm E_a$, we have

$$\frac{1}{l}\sim\frac{2\pi}{\hbar v}V^2\rho_a(E_F), \tag{23}$$

where ρ_a is the density of states per atom in the perfect crystal and v is some average of the group velocity over the Fermi surface. With a bandwidth of $12|\gamma|$, and in view of the roughly triangular shape of the band, we put $\rho_a(E_F)\sim1/(6|\gamma|)$. In the perfect crystal, the band energy is given by $E(\mathbf{k})=-2|\gamma|(\cos k_x a+\cos k_y a+\cos k_z a)$, and the group velocity is $\mathbf{v}=(2|\gamma|a/\hbar)(\sin k_x a,\sin k_y a,\sin k_z a)$. To estimate v we take the point $k_x a=k_y a=k_z a=\pi/2$ on the surface $E(\mathbf{k})=0$, close to our $E_F=-0.1|\gamma|$. This gives $l\sim6\sqrt{3}\gamma^2 a/(\pi E_a^2)\sim3a$. With $N=43$, the relation $s_O\sim r/Nl$ gives $s_O\sim0.009r/a$. The localization length can be estimated as $\xi\sim Nl\sim100a$. Therefore, roughly, the calculated resistance R between the reservoirs should start from $R_0=r/N=r/43$, then rise linearly with the above slope, reaching a value of about $1r$ for sample length $L=100a$, when deviations from linearity should become apparent. Beyond that point, it is the quantity $\ln(R/r)$ that may be expected to increase linearly with L.

Now an impure wire is grown up to a length of $350a$, and the resistance is calculated at every length on the way. Figure 3 shows plots of R/r versus L (lower panel) and $\ln(R/r)$ versus L (upper panel). The curves correspond roughly to the above estimates, but exhibit significant fluctuations, showing the need for averaging over different realizations of the disorder.

Due to interference, quantum-mechanically individual elastic (phase-coherent) resistors do not generally add in series, and the conductance and the resistance, as a function of the length of a disordered conductor, are not self-averaging quantities.[26] In the Ohmic regime, disordered elastic conduc-

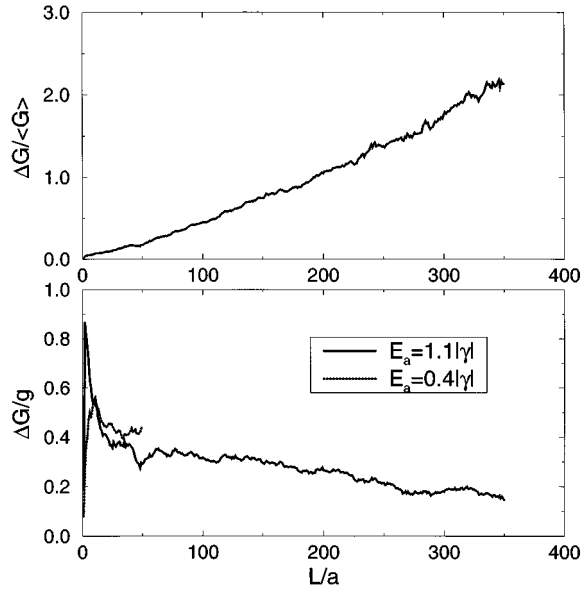

FIG. 4. ΔG in units of $g=2e^2/h$ (lower panel) and $\Delta G/\langle G\rangle$ (upper panel) versus sample length L in units of a. The wire cross section is 8×8 atoms and $E_F=-0.1|\gamma|$ with $N=43$. The sample has random on-site energies of $\pm 1.1|\gamma|$. The averaging is over 150 configurations for each sample length. The lower panel also shows data for sample on-site energies of $\pm 0.4|\gamma|$, with averaging over 100 configurations, for comparison.

tors are expected to show universal conductance fluctuations of root mean square value $\Delta G=\sqrt{\mathrm{Var}G}$, where Var stands for variance, of the order of $g=2e^2/h$.[26] Thus the relative fluctuation $\Delta G/\langle G\rangle$ increases with length. Upon passage into the localization regime, ΔG decreases, while $\Delta G/\langle G\rangle$ diverges with length.[26]

Now the calculation on the 8×8 atom wire is repeated with the same parameters as before. This time, however, for each sample length, G is calculated for 150 different configurations (realizations of the disorder). The specific implementation of the calculation is the following. As an individual sample is grown from $L=1a$ to $L=350a$, G is calculated at every length on the way, and the values are stored. This is done for 150 different samples, producing sets of 150 conductance values for each length.

Figure 4 shows plots of $\Delta G/g$ (lower panel) and $\Delta G/\langle G\rangle$ (upper panel) versus L. The plot of ΔG for $E_a=1.1|\gamma|$ shows a sharp peak at about $L=3a$, close to the estimated mean free path. Peaks in ΔG around $L=l$ have been seen in many test calculations, in which the mean free path l is smaller than the transverse dimension of the wire d. For $l>d$, on the other hand, the peaks are generally suppressed. An example may be seen in Fig. 4 (lower panel), which also shows data for $E_a=0.4|\gamma|$ with $l\sim 20a$. Beyond the peak, ΔG stays between $0.3g$ and $0.4g$ for a while, and, beyond $L\approx 80a$, it decreases smoothly into the localization regime. At the same time, the relative fluctuation $\Delta G/\langle G\rangle$ increases steadily and rises above unity, at which stage $\langle G\rangle$ is no longer a well-defined quantity.

Consider now the quantity $\ln(G/g)$. Figure 5 shows a plot of $\Delta\ln(G/g)/|\langle\ln(G/g)\rangle|^{1/2}$ versus L. The origin of the divergent peak at around $L=80a$ is instructive. As L increases, G decreases, and at some point it reaches a value of about

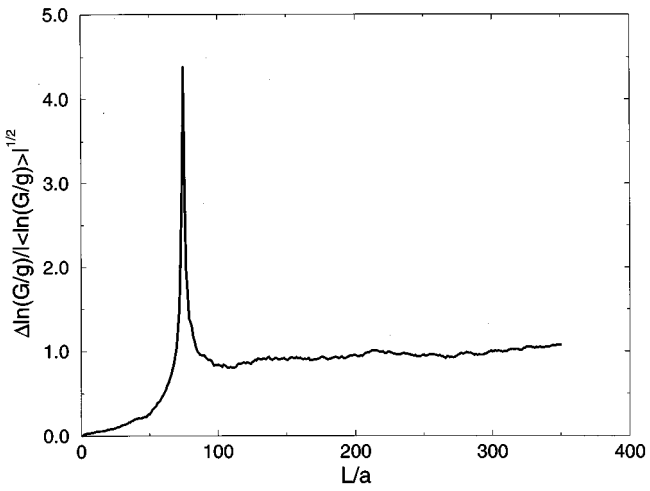

FIG. 5. $\Delta\ln(G/g)/|\langle\ln(G/g)\rangle|^{1/2}$ versus sample length L in units of a. The wire cross section is 8×8 atoms and $E_F=-0.1|\gamma|$ with $N=43$. The sample has random on-site energies of $\pm 1.1|\gamma|$. The averaging is over 150 configurations for each sample length.

$1g$. At that point, $\ln(G/g)$ vanishes and $\Delta\ln(G/g)/|\langle\ln(G/g)\rangle|^{1/2}$ becomes singular. But the point at which $R\sim r$ and $G\sim g$ is roughly the point of transition from the Ohmic to the localization regime [at that point, for large N, the term R_0 in Eqs. (3) and (7) is negligible]. Thus the divergence of $\Delta\ln(G/g)/|\langle\ln(G/g)\rangle|^{1/2}$, and hence of $\Delta\ln(G/g)/|\langle\ln(G/g)\rangle|$ [the relative fluctuation of $\ln(G/g)$], gives a rough indication of the transition between the two regimes. Figure 5 shows that beyond the peak $\Delta\ln(G/g)/|\langle\ln(G/g)\rangle|^{1/2}$ stays approximately constant. Therefore, in that region, the relative fluctuation of $\ln(G/g)$, $\Delta\ln(G/g)/|\langle\ln(G/g)\rangle|$, decreases as $1/|\langle\ln(G/g)\rangle|^{1/2}$. Thus, in the localization regime, the quantity $\ln(G/g)$, as a function of length, is a self-averaging quantity in the usual sense.[26] Estimates of the localization length should be made from plots of $\langle\ln(G/g)\rangle$ or $\langle\ln(R/r)\rangle$ versus L.

In the proposed calculations of the bulk resistivity, we require the slope of R versus L in the Ohmic regime. An ambiguity now arises as to what quantity should be averaged in order to obtain the respective plot. In particular, due to the statistical spread of the calculated values, the quantities $\langle R\rangle=\langle 1/G\rangle$ and $1/\langle G\rangle$ are generally different. However, in the Ohmic regime the fractional difference between them is typically very small. This may be seen visually in Fig. 6, which shows plots of $\langle R\rangle/r$, $g/\langle G\rangle$, and $\exp\langle\ln(R/r)\rangle$. Differences become apparent for $L>30a$, with $\langle R\rangle/r$ being the highest, $g/\langle G\rangle$ the lowest, and $\exp\langle\ln(R/r)\rangle$ in the middle. However, there is no discernible difference in the region $R/r<1/4$, which was taken earlier as the linear regime, within a 1% tolerance level. In this region, the question of what quantity should be averaged is academic.

In the resistivity calculations, the R versus L plots will be prepared from the quantity $\langle R\rangle$, over that range of lengths for which typically $\Delta R/\langle R\rangle<0.1$. The fractional difference between $\langle R\rangle$ and $1/\langle G\rangle$, which is of order $(\Delta R/\langle R\rangle)^2$, is then less than 1%. This range typically corresponds to R values less than $r/5$. Both the slight ambiguity in the construction of

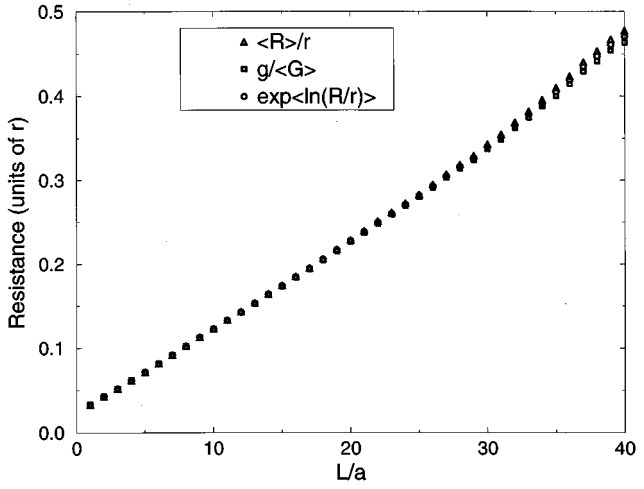

FIG. 6. Plots of $\langle R\rangle/r$, $g/\langle G\rangle$, and $\exp\langle\ln(R/r)\rangle$ versus sample length L in units of a. The wire cross section is 8×8 atoms and $E_F=-0.1|\gamma|$ with $N=43$. The sample has random on-site energies of $\pm1.1|\gamma|$. The averaging is over 150 configurations for each sample length.

the R versus L plots and the deviations from linearity are systematic sources of uncertainty in the estimated Ohmic slopes and corresponding resistivities. In view of the above values, we take 1% as the level of accuracy in the estimate of these quantities.

C. Transition from the Ohmic to the localization regime

Here we compare the results for the 8×8 atom wire with relation (7). Figure 7 shows a plot of $\langle R\rangle/r$ together with the line of best fit (lower panel), and a plot of $\langle\ln(R/r)\rangle$ (upper panel), versus L. The y intercept on the resistance plot corresponds to the term R_0 in Eqs. (3) and (7). The resistance plot gives $s_O=0.0101r/a$. Then $s_O=r/Nl$ gives $l\sim2.3a$, in rough agreement with the earlier estimate. From the slope of the linear region of the logarithmic plot we obtain a localization length of $\xi=61.7a$. The constant c from Eq. (5) becomes $c=s_O\xi/r\approx0.62$. The function $R=rc\sinh(L/\xi)+R_0$, Eq. (7), is now compared with the actual results and with the possible relation $R=rc[\exp(L/\xi)-1]+R_0$, discussed in Sec. II. The lower panel in Fig. 8 shows plots of $\langle R\rangle/r$, $c\sinh(L/\xi)+R_0/r$, and $c[\exp(L/\xi)-1]+R_0/r$ versus L in the Ohmic regime, and the upper panel shows plots of $\exp\langle\ln(R/r)\rangle$, $c\sinh(L/\xi)+R_0/r$, and $c[\exp(L/\xi)-1]+R_0/r$ versus L over a wider range of sample lengths, well into the localization regime. The relation $R=rc\sinh(L/\xi)+R_0$ produces a good fit to the data over the entire range of sample lengths. The form $R=rc[\exp(L/\xi)-1]+R_0$, on the other hand, has the right initial slope but quickly rises above the calculated points.

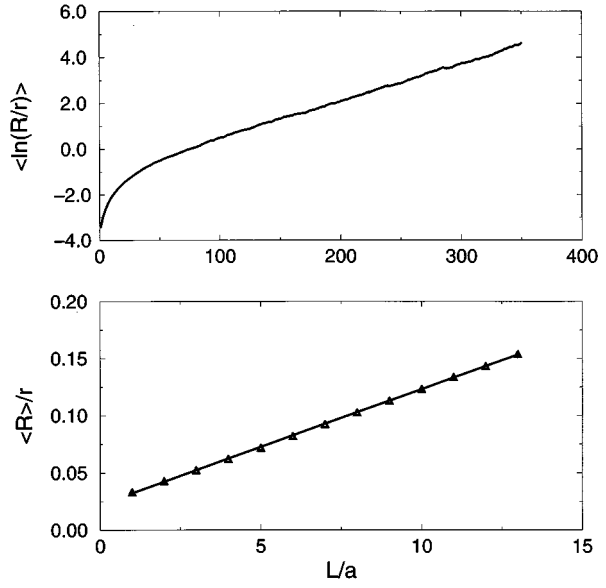

FIG. 7. Plots of $\langle R\rangle/r$ together with the line of best fit (lower panel) and $\langle\ln(R/r)\rangle$ (upper panel), versus sample length L in units of a. The wire cross section is 8×8 atoms and $E_F=-0.1|\gamma|$ with $N=43$. The sample has random on-site energies of $\pm1.1|\gamma|$. The averaging is over 150 configurations for each sample length.

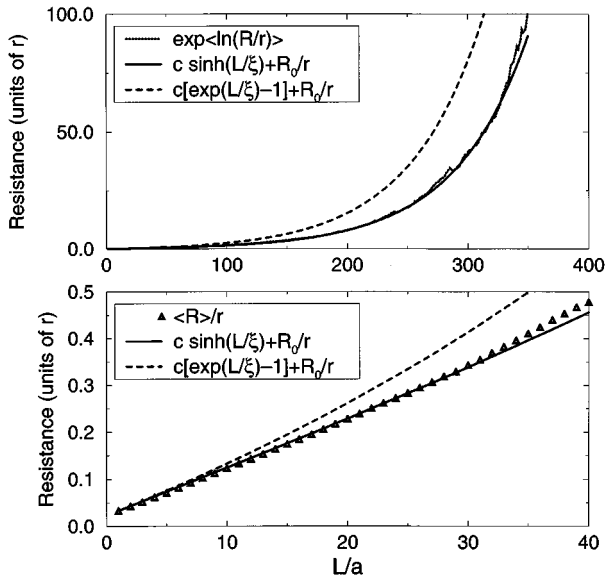

FIG. 8. $\langle R\rangle/r$ (lower panel) and $\exp\langle\ln(R/r)\rangle$ (upper panel), together with $c\sinh(L/\xi)+R_0/r$ and $c[\exp(L/\xi)-1]+R_0/r$, versus sample length L in units of a. From the data, $\xi=61.7a$, $c=0.0101\times61.7$, $R_0/r=1/N=1/43$. The wire cross section is 8×8 atoms and $E_F=-0.1|\gamma|$. The sample has random on-site energies of $\pm1.1|\gamma|$. The averaging is over 150 configurations for each sample length.

Test calculations have been performed for a variety of Fermi energies and wire cross sections, typically with $N>30$, and with different amounts and types of disorder. These include further cases of the present alloylike disorder, the Anderson model with continuously distributed random on-site energies, and intersite disorder. All calculations have produced values of c [Eq. (5)] within several percent of 0.6. The relation $R=rc\sinh(L/\xi)+R_0$ consistently produces good fits to the data.

D. Convergence of the estimated bulk resistivity

The $\langle R\rangle$ versus L plot in Fig. 7 gave an Ohmic slope of $s_O=0.0101r/a$. The cross section of the wire contains 64 atoms. With an area of a^2 per atom, the cross-sectional area of the wire is $A=64a^2$, and the estimated bulk resistivity of the alloy is $\rho=As_O=0.646ra$. Now we vary the cross sec-

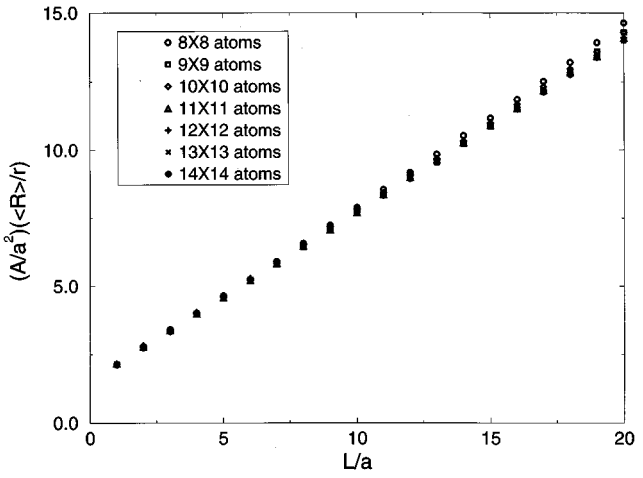

FIG. 9. Plots of $\langle R\rangle/r$, multiplied by the number of atoms A/a^2 in the wire cross section, for cross sections of 8×8, 9×9, 10×10, 11×11, 12×12, 13×13, and 14×14 atoms, versus sample length L in units of a. The sample has random on-site energies of $\pm1.1|\gamma|$ and $E_F=-0.1|\gamma|$. The averaging is over 150 configurations for the 8×8 atom wire and over 50 configurations for the rest.

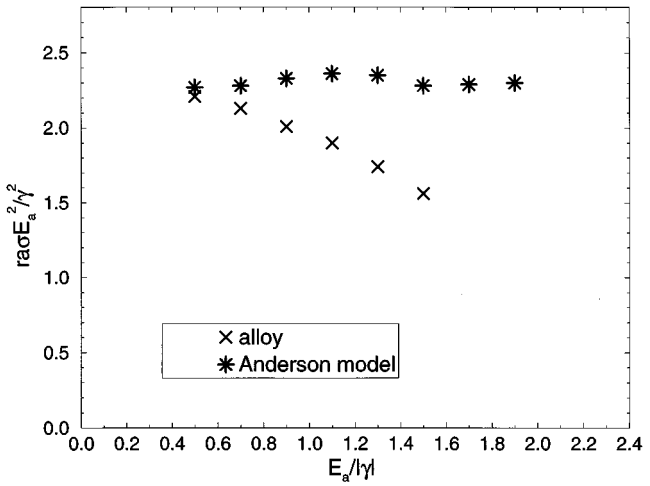

FIG. 10. Calculated values of $ra\sigma E_a^2/\gamma^2$ versus $E_a/|\gamma|$ for a random alloy with on-site energies of $\pm E_a$ and for an Anderson model with on-site energies continuously distributed in the interval $(-3^{1/2}E_a,+3^{1/2}E_a)$. The wire cross section is 10×10 atoms, $E_F=-0.1|\gamma|$, and $N=64$.

tion of the wire. Figure 9 shows plots of the calculated average resistance, multiplied by the number of atoms in the wire cross section, for cross sections of 8×8, 9×9, 10×10, 11×11, 12×12, 13×13, and 14×14 atoms. The slopes give the respective estimates of the bulk resistivity, in units of ra. The respective values are 0.646, 0.626, 0.634, 0.629, 0.630, 0.625, 0.625. As may be expected, the estimate of ρ decreases as the wire cross section increases. It appears to do so in an oscillatory fashion, even though the oscillations lie within the 1% level of accuracy assumed earlier. In the present case, the convergence is very good. Due to the finite-size effects, discussed in the Introduction, it should generally become less so with increasing l/d. In principle, one must study ρ as a function of A by some systematic procedure, such as fitting the calculated values to some asymptotic form, but such analysis will not be done here.

V. TWO EXAMPLES

This section gives two examples of the possible applications of the present calculations. The examples refer to the cases of on-site disorder and interfacial roughness.

A. On-site disorder

This example is a comparison between two different forms of on-site disorder—the alloylike disorder from the preceding section and the Anderson model with continuously distributed on-site energies. Equation (23) would suggest that at least in the weak-scattering limit, for which it was written, the mean free path and the conductivity are inversely proportional to the mean square fluctuation of the on-site energy. In the comparison, the on-site energies for the alloy are set randomly to $+E_a$ or $-E_a$, while for the Anderson model these energies are given a uniform continuous distribution in the interval $(-E_a\sqrt{3},+E_a\sqrt{3})$, with the same mean square fluctuation E_a^2 in each case. The hopping integrals in the sample are the same as in the perfect leads.

The bulk resistivity ρ and the conductivity $\sigma=1/\rho$ are calculated for a range of values of E_a. The cross section of the wire is 10×10 atoms. E_F is set to $-0.1|\gamma|$ as before. There are $N=64$ open channels in the perfect wire. The averaging is over 50 configurations for each sample length.

Figure 10 contains plots of $ra\sigma E_a^2/\gamma^2$ versus $E_a/|\gamma|$ for each type of on-site disorder. In the far left region, the two curves converge, confirming the expectation that in the weak-scattering limit the conductivity is determined by the mean square fluctuation of the on-site energy, and is insensitive to the precise form of the underlying distribution. For the leftmost point on both plots, with $E_a/|\gamma|=0.5$, the mean free path estimate (from $s_O=r/Nl$) is $l\sim14a$.

As $E_a/|\gamma|$ increases, the curve for the alloy descends below that for the Anderson model. This observation can be understood qualitatively as follows. The random alloy consists of small globules of atoms of each kind. These globules have sharp boundaries, giving rise to strong scattering. For the Anderson model one can visualize analogous globules but with softer boundaries, giving rise to weaker scattering. The difference between the two plots shows that as the disorder increases, higher moments of the on-site energy distribution become important.

The results show also that for the Anderson model the relation $\sigma E_a^2=\text{const}$ is very robust. For this model, $ra\sigma E_a^2/\gamma^2$ stays constant to within about 2% over the entire range of $E_a/|\gamma|$. For the rightmost point, with $E_a/|\gamma|=1.9$, the mean free path estimate is $l\sim a$. Thus the above relation remains valid to the point when the mean free path becomes comparable to the lattice parameter and the usual picture of metallic conduction begins to break down.

With $a=3\times10^{-10}$ m, for the point $E_a/|\gamma|=1.9$ in the Anderson model we find $\sigma\approx1640\ \Omega^{-1}\text{cm}^{-1}$. The rightmost calculated point for the alloy has $E_a/|\gamma|=1.5$ with $l\sim1.1a$. With $a=3\times10^{-10}$m, at that point $\sigma\approx1790\ \Omega^{-1}\text{cm}^{-1}$. It would be very interesting to extend both curves further to the right in order to look for the metal-insulator transition,[27] in which the electronic states in the

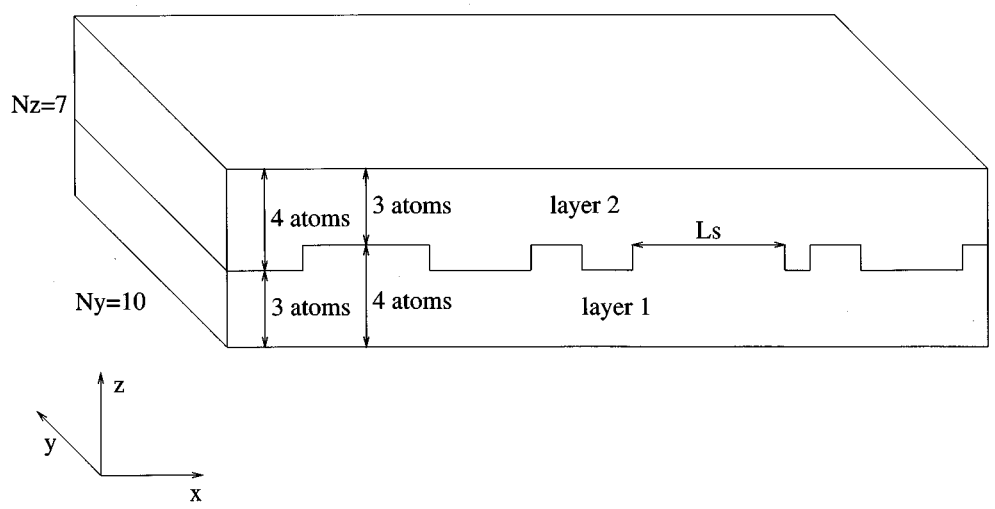

FIG. 11. The geometry of the sample for the interfacial roughness calculations. The details are explained in the main text.

bulk itself become localized and the bulk conductivity vanishes. Unfortunately, such extensions would be difficult at present. The reason is that as l decreases, the localization length in the wire shrinks accordingly, and it becomes necessary to increase the wire cross section so as to obtain a reasonable Ohmic regime. At present, this makes the calculations too slow.

B. Interfacial roughness

In recent years, the problem of transport in magnetic multilayers has received much attention in the context of the giant magnetoresistance effect.[15] One source of complexity in this problem is the possible simultaneous presence of two separate scattering mechanisms—one associated with the interfaces between the layers, and one associated with bulk defects in the layers. The present calculations make it possible to study such combinations of scattering mechanisms. Here we consider the example of a metallic bilayer with geometrical roughness at the interface between the two layers, without and with additional bulk impurities.

The geometry for the sample is shown in Fig. 11. The sample has $N_y=10$ atoms in the transverse y direction and $N_z=7$ atoms in the transverse z direction. The two layers of the sample differ by their on-site energy, which is set to $-1.5|\gamma|$ in layer 1 and $+1.5|\gamma|$ in layer 2. The on-site energy in the leads is zero, as before, and all hopping integrals are equal to γ. The interface between the layers has steps in the longitudinal x direction. The height of each step is one atom. The thickness of layer 1 (layer 2) changes between three atoms (four atoms) and four atoms (three atoms) from step to step. The length $L_s=na$, where n is an integer, of the steps is random. The probability distribution for n is given by $P(n)=q(1-q)^{n-1}$, $0<q<1$, with an average step length of $\langle L_s\rangle=a/q$.

In the present case, the electronic structure of the sample is intrinsically different from that of the perfect leads, even in the absence of any disorder. This difference gives rise to scattering at the actual lead-sample boundaries and to a corresponding contribution to the resistance between the reservoirs. An example is shown in Fig. 12. The figure gives a plot of $\langle R\rangle/r$ versus sample length for the case $q=0.4$, $\langle L_s\rangle=2.5a$. The Fermi energy is $E_F=-0.1|\gamma|$ and the averaging is over 100 configurations per length. The number of open channels in the leads is $N=46$. Extrapolation of the plot to $L=0$ gives a y intercept that exceeds considerably the value $R_0/r=1/46=0.022$ for the resistance between the reservoirs in the absence of the sample. The extra resistance is due to the scattering at the lead-sample boundaries. This additive resistance is immaterial if one is interested in the slope of the plot but could be very important if one were performing calculations for a fixed sample length.

The quality of the plot in Fig. 12 is poorer than before. In the roughness calculations without bulk impurities, it was found that for a given $\langle R\rangle$ the calculated resistances have a bigger scatter than in the earlier examples, with correspondingly less accurate estimates of the Ohmic slopes. The addition of bulk impurities greatly improves the plots.

The calculation is now done for different values of $\langle L_s\rangle$, with and without bulk impurities. The impurity atoms have a concentration of 5% and an on-site energy of $+3|\gamma|$, and are randomly distributed throughout the sample. Figure 13 shows the calculated $R-L$ Ohmic slopes as a function

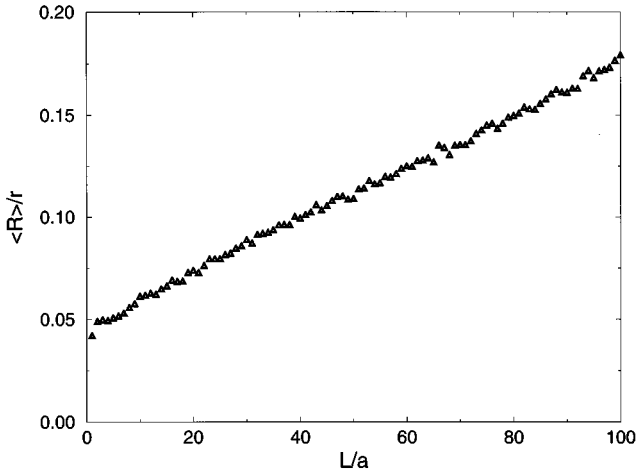

FIG. 12. $\langle R\rangle/r$ versus sample length L in units of a for the case of interfacial roughness with $q=0.4$, $\langle L_s\rangle=2.5a$. The two layers of the bilayer have on-site energies of $-1.5|\gamma|$ and $+1.5|\gamma|$, respectively, and $E_F=-0.1|\gamma|$. The averaging is over 100 configurations for each sample length.

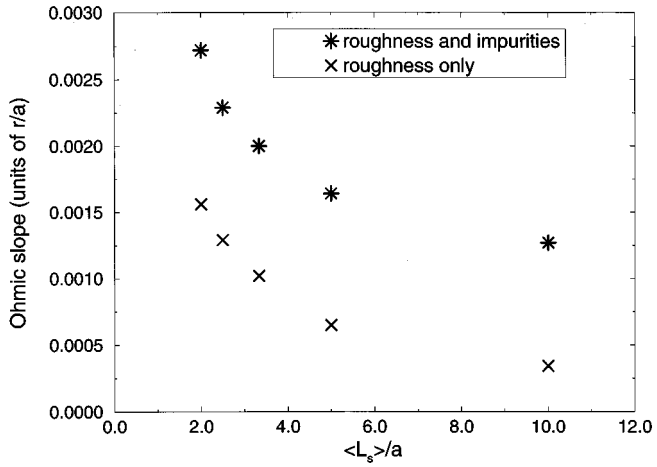

FIG. 13. The calculated $R-L$ Ohmic slopes versus the average length $\langle L_s \rangle$ of the roughness steps, in units of a, for the cases of interfacial roughness without and with additional impurity scattering. The two layers of the bilayer have on-site energies of $-1.5|\gamma|$ and $+1.5|\gamma|$, respectively, and $E_F=-0.1|\gamma|$. The concentration of the impurities is 5% and their on-site energy is $+3|\gamma|$.

$\langle L_s \rangle$, with and without the impurities. The two plots have an approximately constant relative shift, suggesting that the two scattering mechanisms effectively add in series. In another sense, the impurity scattering partially masks the interfacial scattering and decreases its relative contribution to the total resistivity of the structure.

VI. CONCLUSIONS

The purpose of this paper is to present the calculations and their application to the study of conduction in various disordered materials. The method, which is also applicable to one- and two-dimensional structures, can be implemented for a wide range of types and amounts of disorder, while the scattering by the disorder is always treated exactly. One possible use of these calculations is the evaluation of the bulk resistivity of disordered materials. In view of the finite-size effects discussed earlier, such resistivity calculations require small electron wavelengths and small mean free paths. The method would generally not be suitable for Fermi energies near the band edges or for cases of weak scattering. The deviations from Ohmic behavior, due to localization, limit the range of sample lengths from which the respective Ohmic slopes are obtained. In this respect, the sinh function in Eqs. (7) and (8), with its long initial linear part, has been most helpful. The justification for using these equations is their empirically established success in reproducing the shapes of the calculated curves. However, these equations require independent analysis. In addition to the bulk resistivity, the calculations can be used to study the statistical behavior of the elastic conductances and resistances of the disordered wires. For example, the peaks in ΔG around $L=l$ (Sec. IV) and their apparent dependence on the value of l/d, which needs further investigation, could potentially be used for classifying short constrictions and for distinguishing between the ballistic and Ohmic regimes in them. There are two further applications of the present calculations that are currently under investigation. The first is a comparison of the resistivities calculated by the present method with results based on the Kubo-Greenwood formalism. The second application is in the modeling of the giant magnetoresistance effect in magnetic multilayers.

ACKNOWLEDGMENTS

The author would like to thank A. M. Bratkovsky, A. P. Sutton, and E. Yu. Tsymbal for many discussions. The calculations for this paper were carried out at the Materials Modelling Laboratory at Oxford University, which is partially funded by the EPSRC under Grant No. GR/H/58278.

APPENDIX: EQUIVALENCE OF THE TWO EXPRESSIONS FOR THE CONDUCTANCE

We wish to establish the equality of the right hand sides of Eqs. (19) and (22) from the main text. First, we note that since $P_1+P_2=1$, we can also write Eq. (21) as $I=-(1/i\hbar)(P_1V-VP_1)$. Then, using Eqs. (15) and (20), we can reduce the problem to that of establishing the equality of the expressions

$$A=\mathrm{Tr}[(G_1^{0-}-G_1^{0+})t^\dagger(G_2^{0-}-G_2^{0+})t] + \mathrm{Tr}[(G_2^{0-}-G_2^{0+})t^\dagger(G_1^{0-}-G_1^{0+})t] \tag{A1}$$

and

$$B=\mathrm{Tr}[(G^- - G^+)(P_2V-VP_2)(G^- - G^+)(P_1V-VP_1)], \tag{A2}$$

where the argument (E_F) in the Green functions and in the t operators has been omitted for simplicity.

Consider the quantity B. Consider the expression inside the trace. First, we expand this expression. Since the terms in the expansion appear inside a trace, we may cyclically permute the operators in these terms. Expanding, and performing some such permutations, for the expression inside the trace in Eq. (A2) we get

$$\begin{aligned} &VG^-P_2VG^-P_1-VG^+P_2VG^-P_1-VG^-VP_2G^-P_1 \\ &\quad +VG^+VP_2G^-P_1-VG^-P_2VG^+P_1+VG^+P_2VG^+P_1 \\ &\quad +VG^-VP_2G^+P_1-VG^+VP_2G^+P_1 \\ &\quad -P_1G^-P_2VG^-V+P_1G^+P_2VG^-V \\ &\quad +P_1G^-VP_2G^-V-P_1G^+VP_2G^-V \\ &\quad +P_1G^-P_2VG^+V-P_1G^+P_2VG^+V \\ &\quad -P_1G^-VP_2G^+V+P_1G^+VP_2G^+V. \end{aligned} \tag{A3}$$

Next, we require the following relations. First, the Dyson equation for the Green functions can be written in the two equivalent forms $G^\pm=G^{0\pm}+G^{0\pm}VG^\pm$ and $G^\pm=G^{0\pm}+G^\pm VG^{0\pm}$. The two together yield the relations

$$G^+=G^{0+}+G^{0+}tG^{0+}, \tag{A4}$$

$$G^-=G^{0-}+G^{0-}t^\dagger G^{0-}. \tag{A5}$$

They also yield the relations

$$G^+V=G^{0+}t, \tag{A6}$$

$$VG^{+}=tG^{0+}, \tag{A7}$$

$$G^{-}V=G^{0-}t^{\dagger}, \tag{A8}$$

$$VG^{-}=t^{\dagger}G^{0-}. \tag{A9}$$

Finally, we have the relations $G_j^{0\pm}=P_jG^{0\pm}=G^{0\pm}P_j$ for $j=1,2$, and $P_1G^{0\pm}P_2=P_2G^{0\pm}P_1=0$. Using all of the above, together with the definition of t in Eq. (17), expression (A3) becomes, after cyclic permutations in some individual terms,

$$\begin{aligned}&-G_1^{0-}tG_2^{0+}t^{\dagger}+G_1^{0-}tG_2^{0-}t^{\dagger}-G_1^{0+}t^{\dagger}G_2^{0-}t+G_1^{0+}t^{\dagger}G_2^{0+}t\\&+G_1^{0+}tG_2^{0+}t^{\dagger}-G_1^{0+}tG_2^{0-}t^{\dagger}+G_1^{0-}t^{\dagger}G_2^{0-}t-G_1^{0-}t^{\dagger}G_2^{0+}t.\end{aligned} \tag{A10}$$

It is easy to check that the trace of the above expression is the same as expression A, Eq. (A1). This completes the proof of the equivalence of Eqs. (19) and (22) from the main text.

[1] P. Erdös and R. C. Herndon, Adv. Phys. **31**, 65 (1982).
[2] J. P. G. Taylor, K. J. Hugill, D. D. Vvedensky, and A. MacKinnon, Phys. Rev. Lett. **67**, 2359 (1991).
[3] K. Nikolic and A. MacKinnon, Phys. Rev. B **47**, 6555 (1993).
[4] T. N. Todorov and G. A. D. Briggs, J. Phys. Condens. Matter **6**, 2559 (1994).
[5] H. Higurashi, S. Iwabuchi, and Y. Nagaoka, Surf. Sci. **263**, 382 (1992).
[6] K. Nikolic and A. MacKinnon, Phys. Rev. B **50**, 11008 (1994).
[7] A. P. Sutton, M. W. Finnis, D. G. Pettifor, and Y. Ohta, J. Phys. C **21**, 35 (1988).
[8] T. N. Todorov, G. A. D. Briggs, and A. P. Sutton, J. Phys. Condens. Matter **5**, 2389 (1993).
[9] P. A. Lee and D. S. Fisher, Phys. Rev. Lett. **47**, 882 (1981).
[10] J. B. Pendry, A. B. Prêtre, P. J. Rous, and L. Martin-Moreno, Surf. Sci. **244**, 160 (1991).
[11] D. J. Thouless, Phys. Rev. Lett. **39**, 1167 (1977).
[12] N. E. Cusack, *The Physics of Structurally Disordered Matter* (Hilger in association with the University of Sussex Press, Bristol, 1987), Chap. 9, Sec. 9.
[13] E. H. Sondheimer, Adv. Phys. **1**, 1 (1952).
[14] J. M. Ziman, *The Physics of Metals* (Cambridge University Press, Cambridge, England, 1969), Chap. 4, Sec. 3.
[15] A. Fert and P. Bruno, in *Ultrathin Magnetic Structure II*, edited by B. Heinrich and J. A. C. Bland (Springer, Berlin, 1994), Chap. 2, Sec. 2.
[16] R. Kahnt, J. Phys. Condens. Matter **7**, 1543 (1995).
[17] M. C. Payne, J. Phys. Condens. Matter **1**, 4931 (1989).
[18] Y. Imry, in *Directions in Condensed Matter Physics*, edited by G. Grinstein and G. F. Mazenko (World Scientific, Singapore, 1986), p. 101.
[19] M. Büttiker, in *Electronic Properties of Multilayers and Low-Dimensional Structures*, edited by J. M. Chamberlain *et al.* (Plenum Press, New York, 1990), p. 51.
[20] B. L. Al'tshuler and P. A. Lee, Phys. Today **41** (12), 36 (1988).
[21] P. W. Anderson, D. J. Thouless, E. Abrahams, and D. S. Fisher, Phys. Rev. B **22**, 3519 (1980).
[22] P. W. Anderson, Phys. Rev. B **23**, 4828 (1981).
[23] Y. B. Band, H. U. Barranger, and Y. Aviashi, Phys. Rev. B **45**, 1488 (1992).
[24] A. V. Tartakovsky, Phys. Rev. B **52**, 2704 (1995).
[25] A. P. Sutton, *Electronic Structure of Materials* (Clarendon Press, Oxford, 1993), Chap. 4.
[26] P. A. Lee, A. D. Stone, and H. Fukuyama, Phys. Rev. B **35**, 1039 (1987).
[27] P. A. Lee and T. V. Ramakrishnan, Rev. Mod. Phys. **57**, 287 (1985).